Synthesis and Characterization of Alumina Powders Obtained at Various Temperatures Via Sol-Gel Method

Hakim Attil[1,2], Ali Aksas[2], Miloud Sebais[1], Ouahiba Halimi[1]

[1]*Laboratoire de Cristallographie, Faculté des Sciences Exactes, Université des Frères Mentouri, Route Ain El Bey, Constantine, Algérie*
[2]*Université de Bejaia, Faculté des Sciences de la Nature et de la Vie, Laboratoire de Biotechnologies Végétales et Ethnobotanique, 06000 Bejaia, Algérie*
Email: hakim.attil@univ-bejaia.dz

Abstract: Alumina powders were synthesized by sol-gel method using aluminum isopropoxide as the precursor, de-ionized water as a solvent and hydrochloride acid as a gelation agent. The alumina gel has been dried and sintered at different temperatures in the range 200°C to 1200 °C. The synthesized samples were characterized by Termogravimetry analysis (TG/DTA), Fourier Transform Infrared Spectroscopy (FTIR), X-Ray diffraction (XRD), N2 adsorption / desorption techniques (BET) and Scanning Electron Microscopy (SEM). The X-ray diffraction diagrams showed the formation of different alumina's phases such as ϒ-alumina obtained between 400°C and 900°C, θ-alumina at 1000°C and finally α-alumina was obtained at 1100°C. According to the calcination temperature, the crystallite size varies between 15.4 and 41.5nm. FT-IR confirmed the presence of hydroxyl groups and Al-O bonding vibrations, the specific surface area was found in the range of 74,939 and 156,3255 m2g-1, the pore diameter was in the range of 6,5579 to 9,4485nm and pore volume varies between of 0,082435 to 0,30514 cm3g-1depending as a function of heat treatment, and finally the SEM images reveal the formation of irregularly shaped particles with a disordered, heterogeneous structure. Likewise, thermal properties were investigated using the thermogravimetric method (TG) and differential thermal analysis (DTA), illustrating the thermal stability of the α-alumina phase at over 1100°C.

Keywords: Aluminium Oxide(Al2O3); Phase transition; sol-gel; Calcinations; XRD;FT-IR;SEM;BET.

1. Introduction

Aluminum oxide with the chemical formula Al_2O_3, and commonly referred to by the generic name of alumina, has important applications in various domains, especially in the field of catalysis, it is used as support for catalysts [1-2-3], in electronic it is employed semiconductors, laser tubes sensors and capacitors owing to its strong electrical permittivity, good thermal conductivity and of its high gap[4-5-6].Alumina has found many applications in the biomedical field, particularly in dental and orthopedic implants because of its biocompatibility and for its low toxicity in the human body [7-8]. It has also been used for other applications such as ballistic armor, sealing rings, corrosion protection [9-10-11-12], reinforcements for composite materials and surface coatings in various fields of industrial

properties due to its exceptional properties such as high electrical insulation, high hardness, good wear resistance, chemical inertness, high melting point (2072°C), high rigidity and its good corrosion resistance[13-14-15-16].

Alumina crystallizes in various crystallographic structures, the more stable phase is α-Al2O3 which has a corundum structure, the other metastable phases (γ-, δ-, θ-, κ-, ε-, η-, χ-Al2O3) are also called transition alumina's due to their appearance before the corundum structure during the dehydration of aluminum hydroxides. Each of the polymorphs alumina is observed in a defined temperature range.

Nano-alumina powders can be synthesized using diverse methods like: Bayer [17], sol-gel [10-11-18], ball milling [19-20], precipitation [21-22] and hydrothermal synthesis [23]. However, some of these methods have disadvantages: ball milling may incorporate impurities, the reactions generated during hydrothermal processes require high temperature and pressure, while the precipitation is complex and requires long washing and aging times [21-23-24].

Among these techniques, the Sol-gel method is the most promising because it has a good control of the sample morphology, texture, and chemical composition can be controlled by monitoring the synthesis parameters. It is also possible to prepare materials in a wide variety of forms: ultra-fine powders of high purity, fibers, solids, aerogels, thin films, and bulk materials at ambient temperatures [25-26].

The aim of this work is elaboration and characterization of alumina powders obtained by sol-gel method using aluminum isopropoxide as a precursor, water as a solvent and hydrochloride acid as gelation agent. The calcination in muffle furnace was performed, at different temperatures ranging from 200 to 1200°C with a pitch of 100°C, to determine the influence of temperature parameter on the crystalline quality of resulting alumina. The resulting materials were characterized by X-Ray diffraction (XRD), to find out crystalline phases, Fourier Transform Infrared Spectroscopy (FTIR) to identify the functional groups in the structure of the powders, The Brunauer-Emmet-Teller (BET) method was applied to calculate the specific surface area, and Scanning Electron Microscopy (SEM) for the observation of the microstructure of the prepared alumina particles.

2. Materials and Methods

2.1. Materials

The sol-gel method was used to prepare alumina powders. The precursor is aluminium isopropoxide (≥98%) $C_9H_{21}AlO_3$ (Sigma Aldrich), the solvent is demineralized water H_2O and hydrochloride acid HCL 36.5-38% concentration (Sigma Aldrich) as gelation agent.

2.2. Preparation of the alumina powders

In a typical synthesis of alumina powder (Al_2O_3), 1 g of $C_9H_{21}AlO_3$ was dissolved in 10 ml of de-ionized water, with magnetic stirring at 80°C for 1h.Hydrochloride acid is added drop-wise into the solution which will remain under stirring for an additional 30min, until it turns to a clear solution. The prepared solution was left to rest until gel formation. The obtained gel has undergone aging to room temperature for 2 days. After that, the samples were dried in thermal oven at 120°Cfor 8 hours and then calcined at 200°C, 300°C, 400°C, 500°C, 600°C, 700°C, 800°C, 900°C, 1000°C, 1100 and 1200 ° C for 3h in a muffle furnace with a temperature ramp of 5°C/min. The obtained powders were characterized by different techniques.

2.3. Characterization techniques

The thermogravimetric method (TG) and differential thermal analysis (DTA) were carried out using LABSYS evo instrument and investigated in nitrogen atmosphere at a heating rate of 5°C/min from room temperature to 1200°C.

The XRD patterns of prepared alumina powders were performed on a Bruker D8 diffractometer using CuKα radiation (λ = 1.542Å) with diffraction angle range 2θ=0° to 80° operating at an acceleration voltage of 40KV and a current of 40mA.The ICCD database was employed to identify the crystalline phase of the samples.

The characteristic vibrations of the molecular bonds and the chemical nature of the samples were demonstrated by Fourier transform infrared spectroscopy (FTIR) using an IR Affinity-1 SHIMADZU type spectrometer. The samples were analyzed in the range 400 $cm^{-1}$to 4000 cm^{-1} at a scan rate of 40 rounds / min for 4 cm^{-1} resolution.

The specific surface area and the pore size distribution of the samples were measured using a N2 adsorption-desorption analyzer on ASAP2020 Micrometrics apparatus. Before test the samples were degassed condition of 250°C for 300min at a ramp rate of 10°C/min. The pore size distribution, average pore diameter and total pore volume were calculated according to the Non-Local Density Functional Theory (NLDFT) method.

The surface morphology was analyzed by scanning electron microscopy (SEM) using Quantum 250 instrument with tungsten filament from the FEI Company.

3. Results and discussion

3.1. Gravimetric and Differential Thermal Analysis (TG-DTA)

Thermal gravimetric analysis (TG-DTA) of the gel dried at 120°Cfor 8 hours was performed and results are displayed in Figure 1. The TG profile shows that mass loss occurs in three stages. The initial weight loss occurs between room temperature and 100 ° C, this weight loss is estimated at 20%, and endothermic peak around 109.46 ° C is observed in the DTA curve which is mainly due to evaporation of water. The second step is observed between 200 ° C and 400 ° C, and the weight loss is estimated at 28%, an endothermic peak around 430 ° C is observed on the DTA curve. This result is due to the decomposition of residual organic matter and the transformation of the crystalline phase. The γ-Al_2O_3 phase is formed by the dehydration reaction of the polycrystalline boehmite according to the reaction equation $2AlOOH \rightarrow Al_2O_3 + H_2O$ [18].Subsequently, no appreciable weight loss was observed in the sample due to the formation of a stable compound that is α-Al_2O_3. However, the DTA curve with a tendency to growth is observed, which indicates the suppression of the phase transformation. This phenomenon is mainly due to the stabilization of the crystalline structure.

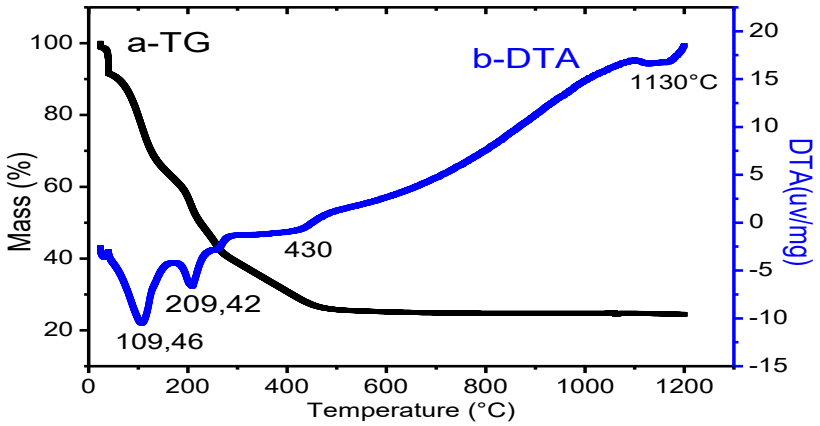

Figure 1. *Thermogravimetric curves a-TG and b-DTA of gel dried at 120°C.*

3.2. X-ray Diffraction (XRD)

The XRD patterns of the powders obtained after calcination at 200°C and 300°C are depicted in Figure 2. Spectra showed peaks at 2θ=13.44°, 28.05°, 37.87°, 49.20° ,54.68° ,64.87° ,71.75° and 85.91°,matching respectively to planes (020), (120), (031), (200), (151), (002), (251), and (311) of boehmite, according to the (JCPDS-00-017-0940) database. The structure of boehmite has orthorhombic symmetry with the space group Amam and lattice parameters

a = 3, 69Å; b=2.24Å and c = 2.86Å.The intensity and the width of XRD peaks indicate that a larger amount of boehmite crystals are formed throughout the samples.

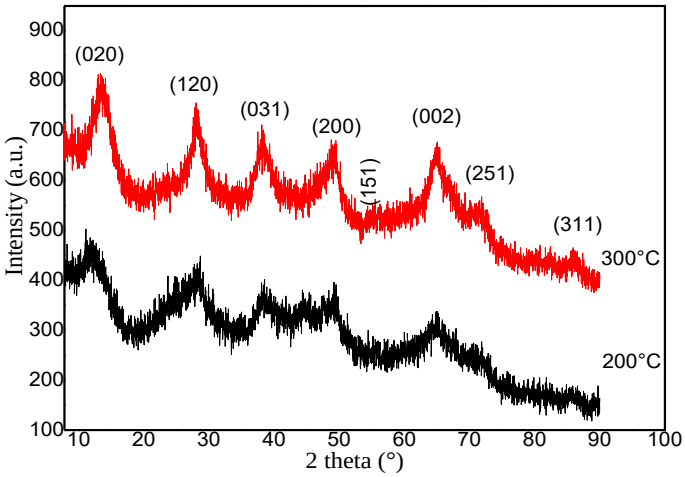

Figure 2. *XRDpatterns of the alumina powders obtained after calcination at 200°C and 300°C.*

The Figure 3 depicts the XRD patterns of the crystalline powders obtained after calcinations at 400,500,600, 700, 800 and 900°C. Spectra reveal peaks at 2θ=19.36, 32.64, 36.78, 39.36 45.51, 60.69, 67,18 and 84,91° associated respectively to the planes (111), (220), (311) (222); (400), (511), (440) and (444)which are assigned to crystals ofγ-Al_2O_3 according to the (JCPDS file-00-010-0425).Thus, the obtained result make it possible to affirm that formed crystals have the cubic structure of γ-Al_2O_3withthe space group Fd3m and lattice parameters a = b = c = 7.90Å. The increase in the temperature of calcinations did not change significantly the position of the peaks, thus indicating that there is no change of the phase structure [28].The observed slight shift expresses a small change in the lattice parameters. From spectra, one can note that the crystalline powders obtained after calcinations at 400°C, 500°C and 600°C have less intense peaks than those obtained with powders calcined at 700, 800 and 900°C which is explained by the enhancement of the degree of crystallization [27-28]. Also the full width at half maximum intensity (FWHM) decreases with calcination temperature which indicates an increase of crystallite size. The threshold temperature to achieve the γ-alumina phase was established at 400°C and the crystallization of this phase continues up to 900°C.

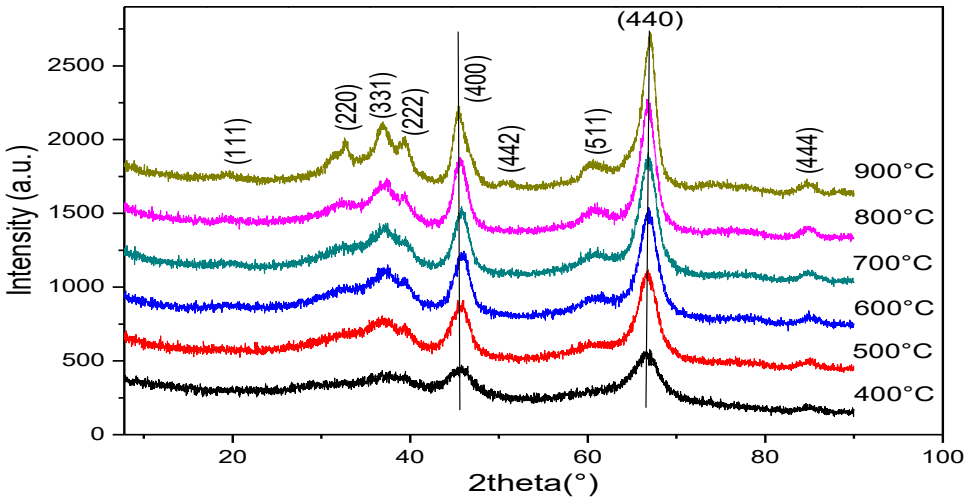

Figure 3. *X-ray diffraction patterns of the crystalline powders obtained after calcination at 400, 500, 600,700,800 and 900°C.*

The θ-alumina phase with monoclinic structure is observed in the sample calcined at 1000°C, whose spectrum is represented in Figure 4. The lattice parameters are a = 5.70 Å, b = 2.92Å and c = 11.90Å according to the (JCPDS file 00-009-0440).

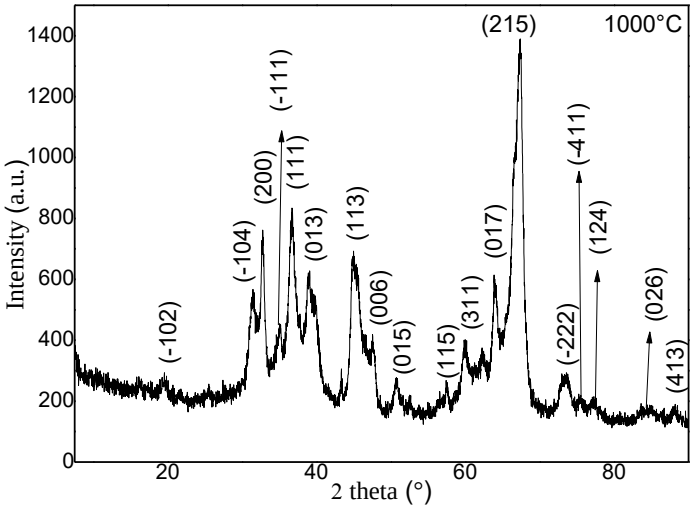

Figure 4. *XRD pattern of the crystalline powder obtained after calcination at 1000°C.*

Likewise, calcinations at 1100 and 1200°C were performed and the XRD spectra of corresponding samples are shown in Figure 5. The increment of the temperature up to 1100°C the precursor has leaded to the crystallization of α-alumina phase and the intensities of peaks have risen and are in agreement with the (JCPDS file 00-042-1468) data of rhombohedral structure. The space group is R3c and lattice parameters are: a = 4.7885Å; b = 4, 7588 Å and c = 12, 9920Å.

Thus, XRD studies indicate the thermodynamically driven phase transformation from $Al(OH)_3$ to AlOOH, γ, θ and α-phases of alumina under the heat treatment from 200°C to 1200°C. The simple annealed at 1200°C show the presence of majority and stable α-phase.

During thermal treatment, the stable α-alumina phase is obtained by a series of phase transformations according to the overall reactions shown below [29]:

$$Al(OC_3H_7)_3 + H_2O \xrightarrow{80°C} Al(OC_3H_7)_2(OH) + C_3H_7(OH) \quad (1)$$

$$2Al(OC_3H_7)_2(OH) + H_2O \xrightarrow{HCl} C_3H_7O - \underset{Al}{\overset{OH}{|}} - O - \underset{Al}{\overset{OH}{|}} - OC_3H_7 + 2C_3H_7OH \quad (2)$$

$$2Al(OH)_3 \xrightarrow{400°C} \gamma - Al_2O_3 + 3H_2O \quad (3)$$

$$\gamma - Al_2O_3 \xrightarrow{1000°C} \theta - Al_2O_3 \xrightarrow{1100°C} \alpha - Al_2O_3 \quad (4)$$

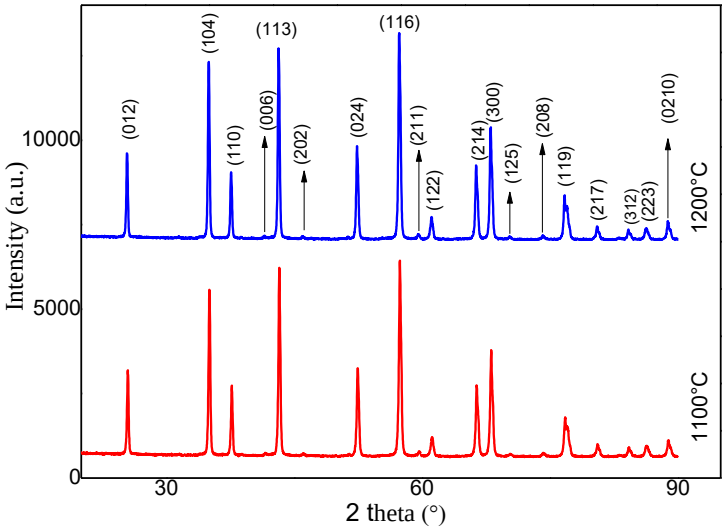

Figure 5. *XRD patterns of the crystalline powders obtained after calcination at 1100 and 1200°C.*

The average crystallite size of the alumina nanoparticles was calculated using Debye-Scherrer formula [24]: $D = 0.9\lambda/\beta \cos(\theta)$ (5)

Where D is the crystallite size, λ wavelength of the X-ray radiation (λ = 1.542Å), θthe Bragg diffraction angle and βthe full width half maximum intensity (FWHM) of the diffraction peak.

The obtained results are given in table 1 .The size values show that the average size of the crystallites increases as a function of the calcinations temperature, it varies between 15,4 nm for treated powders at 200°C and 300°C according to the (020) plane and 41.5 nm for those treated at 1100°C and 1200°C according to the(104) plane.

Table 1. *Size of crystallites calculated with Debye-Scherrer relation*

Température °C	2θ (°)	FWHM(°)	D(size of crystallites)(nm)
200 et 300°C	13,05	0,51	$D_{(020)}$=15,4
400, 500, 600, 700, 800 and 900°C	67,32	0,57	$D_{(440)}$=16,7
1000°C	67,44	0,23	$D_{(215)}$=40,8
1100 et 1200°C	34,90	0,20	$D_{(104)}$=41,5

3.3. Fourier Transform Infrared (FTIR) Analysis

In order to highlight the characteristic alumina groups and bonds and the effect of calcination, the alumina gels prepared at 200°C and 300°Cwere analyzed by FT-IR spectroscopy (Figure 6). For both samples the presence of a broad band at about 3291.97 cm^{-1} and 3303.14 cm^{-1} is attributed to the vibration of the O-H bond due to the added solvent during the hydrolysis or during the condensation process [30-31]. The bands centered at 2104.18 cm^{-1} and 2100.04 cm^{-1} characterize the vibration of the C-H bond of aluminum isopropoxide [32, 33]. The bands at 1635,02 $cm^{-1}$is due to the deformation vibration δ (H-O-H) of the water molecules present in the powder [28, 30, 33] and finally, the signal relating to the vibrations of

the C-O bonds is observed at 1069.05 cm-1 [30, 31, 33]. The Al-O bond is marked by the presence of an absorption band at 469.57 cm^{-1} [34, 35, 36].

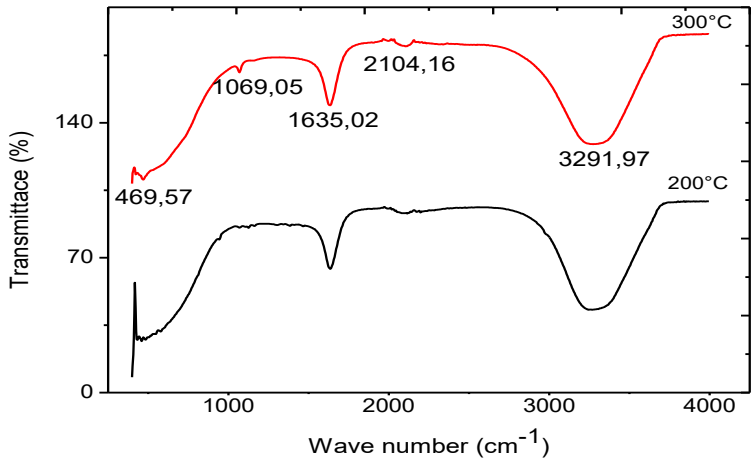

Figure 6. *FT-IR spectra of the alumina powders obtained after calcination at 200°C and 300°C.*

For a calcination treatment superior at 400 ° C (Figure 7), the bands relating to the vibration frequencies of the Al-O bond appear clearly between 400 and 800 cm^{-1}[31,35,37]. At the same time, the bands relating to organic groups disappear. These results are in agreement with the XRD study witch justifies the formation evolution of the transitional phases of alumina and the formation of stable phase of α-alumina.

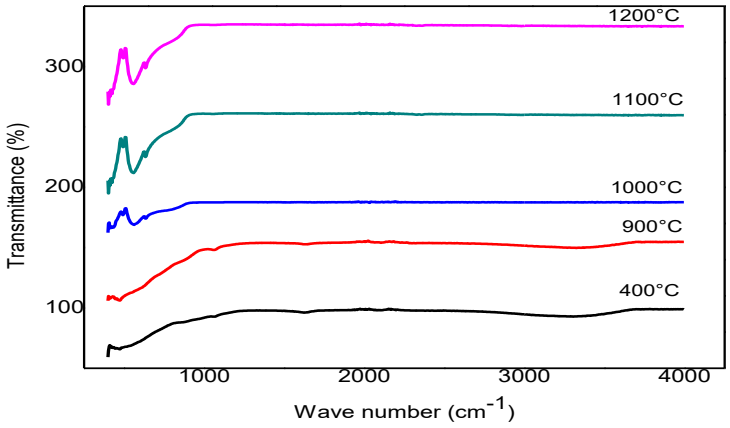

Figure 7. *Infrared spectra of the powders obtained after calcinations at 400°C, 900°C, 1000°C, 1100°C and 1200°C.*

3.4. BET Analysis

The textural properties of the powders synthesized at different calcinations temperatures were determined by the N_2 adsorption-desorption isotherms and to evaluate the pore-size distribution, a further calculation was performed by applying the NLDFT method. The detail analyses of the isotherms are summarized in Figure 8 and table 2.

The International Union of Pure and Applied Chemistry (IUPAC) classified the porous materials on the basis of the pores diameters (r_p). In this category the porous materials are microporous (r_p<2 nm), mesoporous (2 nm<r_p<50 nm) or macroporous (50 nm<r_p) [38].

The nature of the azote adsorption - desorption isotherms of samples synthesized at 900 °C, and 1000 °C and the presence of large hysteresis loops (figure 8-b) at very low pressure of

P/ P0, which to classify the isotherm as type IV, according to the IUPAC classification, characteristics for mesoporous materials [39]. On the other hand for the adsorption-desorption isotherm of the alumina synthesized at 1100 °C in the present study follows the type IV isotherm. In fact, the isotherms obtained do not fit the adsorption and desorption curves and create a hysteresis loop at high relative pressures. The existence of this type of hysteresis loop and type IV isotherm in this sample indicates the mesoporous nature of the synthesized mesoporous alumina [40].

The BET method applied for adsorption isotherm allowed us to calculate the specific surface area table1.To evaluate the pore size distribution another calculation was carried out by applying the model NLDFT, and the results obtained are represented on Figure 8-b.The specific surface area of the sample calcined at 900°C who is from 156,3255 m^2/g is much bigger relative to samples obtained after heat treatment 1000°C and 1100°C attributed to 137,8060 m^2/g and 74,9390 m^2/g respectively. Thermal treatment leads to the decomposition of residual organic groups and the collapse of the lamellar structure, to a volume contraction of the crystals and therefore to a reduction in the specific surface area, despite the loss of mass [38-40].On the other hand, it is clear from the results of Table 1, the pore volumes and pore diameters for the samples alumina obtained after calcinations at 900, 1000 and 1100°C sharply decreases with increasing calcinations temperatures. The pore distribution is in the range of 6.5579 to 9.4485 nm confirming the mesoporous character of the samples synthesized.

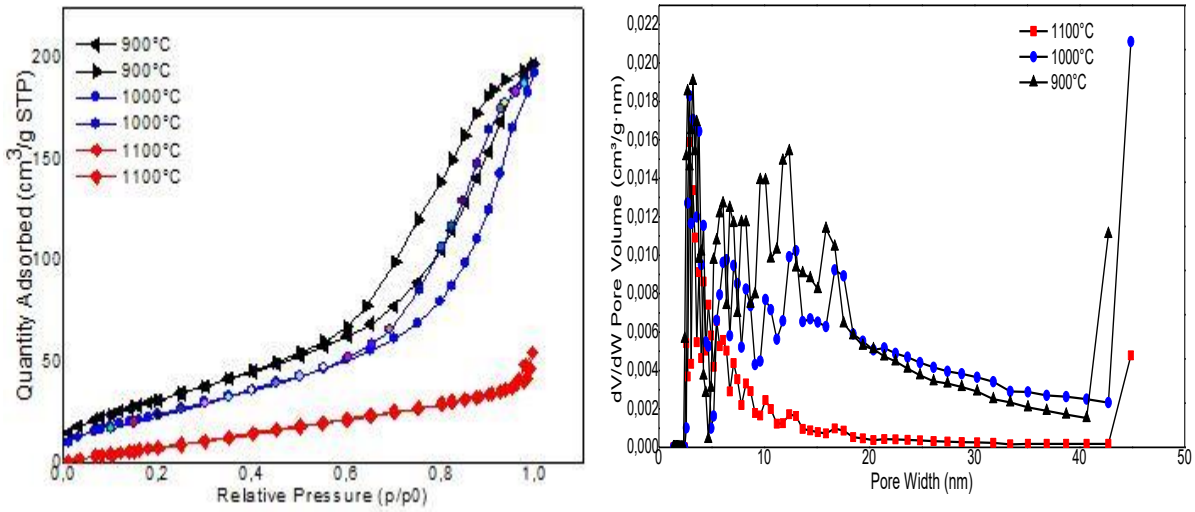

(a) (b)

Figure 8. *(a) Nitrogen adsorption-desorption isotherms and (b) NLDFT pore-size distribution of sample after heat treatment from 900°C to 1100°C.*

Table 2. *Surface area, pore size, and pore volume of synthesized samples*

Samples	Surface area ($m^2\ g^{-1}$)	Pore diameter (nm)	Pore volume ($cm^3\ g^{-1}$)
900°C	156,3255	9.4485	0.305140
1000°C	137,8060	8.4069	0.281555
1100°C	74,9390	6.5579	0.082435

3.5. Scanning electron microscopy

Figure 9 collects the SEM micrograph of the powders obtained at various temperatures of calcinations; 900°C, 1000°C, and 1100°C. The SEM images in Figure 9(a_1,b_1,c_1) show the formation of irregularly shaped particles with a disordered and heterogeneous rough surface structure with a narrower particle size distribution at the micrometer scale with an average size of 60µm - 110µm,however Figure 9(a_2,b_2) highlights the presence of irregularly shaped particles which are in the 3µm and 800nm range, it is also clear that 1100°C Figure 9(c_2), the

grains are then well defined and better formed in a homogeneous manner ,the average crystallite sizes were 130 and 200 nm correspond to the alumina phase α-Al2O3 .These results also confirms the polycrystalline nature of α-Al2O3 particles, which are in consistent with the published results.

The elementary chemical composition of the synthesized samples was examined using EDX (Energy Dispersive X-ray spectroscopy). Quantitative measurement results obtained from EDX analysis (Figure.10) reveal the presence of Al and O with percentage weight of 38, 11% and 61, 89 %, respectively. The presence of higher percentage weight of oxygen can be traced to the formation of Al_2O_3 in the powders obtained after calcinations superior or equal to 400°C.

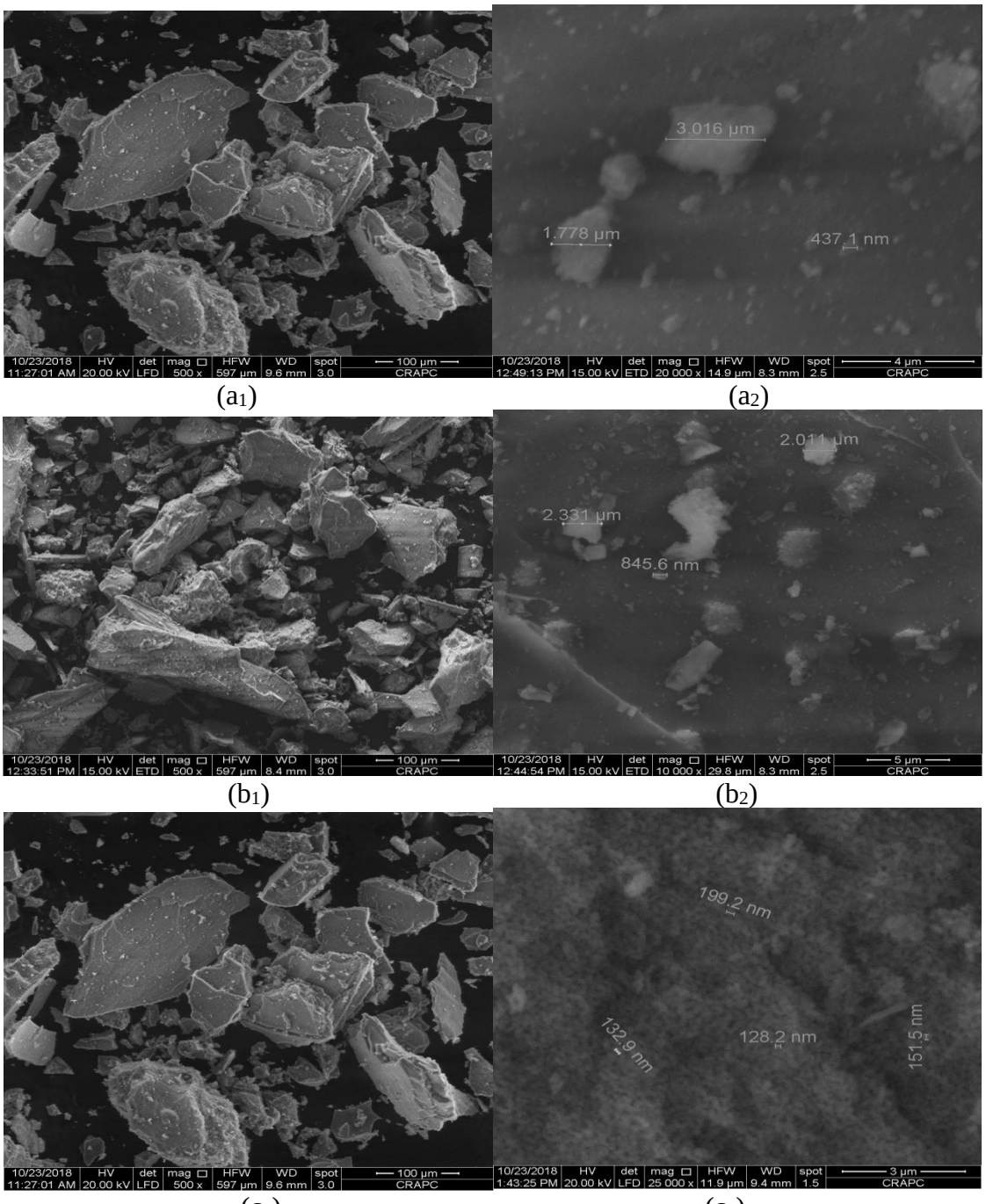

(a_1) (a_2)

(b_1) (b_2)

(c_1) (c_2)

Figure 9. *SEM micrograph of the powders obtained after calcinations at different temperatures: (a_1, a_2) 900°C, (b_1, b_2) 1000°C and (c_1, c_2) 1100°C.*

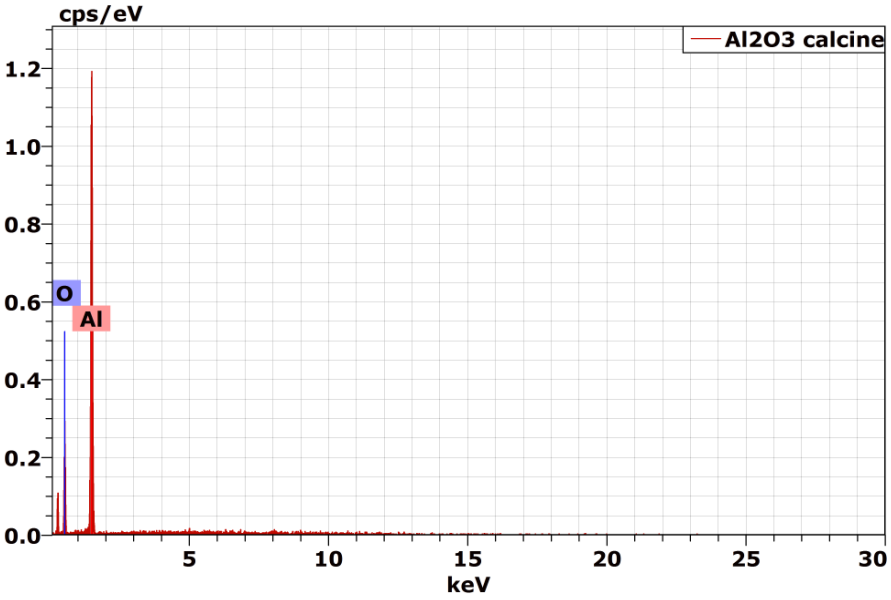

Figure 10. *EDX spectrum of Al_2O_3 sample at 1100°C.*

4. Conclusion

This work consists of preparation powders of alumina obtained at different temperatures calcinations from the dried gel by using the sol-gel process. The results obtained from the XRD show the formation of three crystallized phases in various forms, the conversion to transition alumina gave a γ-alumina phase of cubic structure is obtained in the range 400 ° C and 900°C, applying a heat treatment at temperatures higher than 1000°C leads to obtaining crystalline θ-alumina phase and finally, the most thermodynamically stable phase α-alumina phase of rhombohedral structure, is observed at 1100 ° C. The effect of calcinations temperature on the average crystallite size was investigated. It was found that the average crystallite size alumina obtained at low calcination temperature was smaller than that obtained from high calcination temperature determined by the Debye-Scherrer formula. While the functional surface groups of Al_2O_3 were confirmed by Fourier transform infrared spectroscopy (FT-IR).The SEM images show that the synthesized powders are composed of small irregularly shaped particles of a few micrometers in size. EDX analysis reveals the presence of Al and O confirming the formation of alumina. The Sol-gel method has shown great efficiency for the synthesis of different alumina phases.

References

1. Klapötke, T. M., McMonagle, F., Spence, R. R., & Winfield, J. M. (2006). γ-Alumina-supported boron trifluoride : Catalysis, radiotracer studies and computations. Special 2006 ACS Award Issue ": For Creative Work in Fluorine, 127(10), 1446-1453. https://doi.org/10.1016/j.jfluchem.2006.05.010
2. Looi, P. Y., Mohamed, A. R., & Tye, C. T. (2012). Hydrocracking of residual oil using molybdenum supported over mesoporous alumina as a catalyst. Chemical Engineering Journal, 181-182, 717-724. https://doi.org/10.1016/j.cej.2011.12.080
3. Newnham, J., Mantri, K., Amin, M. H., Tardio, J., & Bhargava, S. K. (2012). Highly stable and active Ni-mesoporous alumina catalysts for dry reforming of methane. 10th International Conference on Clean Energy 2010, 37(2), 1454-1464. https://doi.org/10.1016/j.ijhydene.2011.10.036

4. Cimpoiasu, E., Tolpygo, S. K., Liu, X., Simonian, N., Lukens, J. E., Likharev, K. K., Klie, R. F., & Zhu, Y. (2004). Aluminum oxide layers as possible components for layered tunnel barriers. Journal of Applied Physics, 96(2), 1088-1093. https://doi.org/10.1063/1.1763229
5. Kushmerick, J. (2009). Molecular transistors scrutinized. Nature, 462(7276), 994-995. https://doi.org/10.1038/462994a
6. Vieira, E. M. F., Levichev, S., Dias, C. J., Igreja, R., Buljan, M., Bernstorff, S., Conde, O., Chahboun, A., Rolo, A. G., & Gomes, M. J. M. (2013). Charge storage behavior of nanostructures based on SiGe nanocrystals embedded in Al2O3 matrix. The European Physical Journal B, 86(7), 336-. https://doi.org/10.1140/epjb/e2013-40124-2
7. Thamaraiselvi, T. V., & Rajeswari, S. (2004). Biological evaluation of bioceramic materials—A review. Trends in Biomaterials and Artificial Organs, 18(1), 9+.
8. Rahman, H. S. A., Choudhury, D., Osman, N. A. A., Shasmin, H. N., & Abas, W. A. B. W. (2013). In vivo and in vitro outcomes of alumina, zirconia and their composited ceramic-on-ceramic hip joints. Journal of the Ceramic Society of Japan, 121(1412), 382-387. https://doi.org/10.2109/jcersj2.121.382
9. Ćurković, L., Jelača, M. F., & Kurajica, S. (2008). Corrosion behavior of alumina ceramics in aqueous HCl and H2SO4 solutions. Corrosion Science, 50(3), 872-878. https://doi.org/10.1016/j.corsci.2007.10.008
10. Singh, I. B., Gupta, P., Maheshwari, A., & Agrawal, N. (2015). Corrosion resistance of sol–gel alumina coated Mg metal in 3.5 % NaCl solution. Journal of Sol-Gel Science and Technology, 73(1), 127-132. https://doi.org/10.1007/s10971-014-3503-5
11. Nofz, M., Zietelmann, C., Feigl, M., Dörfel, I., & Saliwan Neumann, R. (2015). Microstructural origin of time-dependent changes in alumina sol–gel-coated Inconel 718 exposed to NaCl solution. Journal of Sol-Gel Science and Technology, 75(1), 6-16. https://doi.org/10.1007/s10971-015-3668-6
12. Jiang, X., Ishizumi, A., Suzuki, N., Naito, M., & Yamauchi, Y. (2012). Vertically-oriented conjugated polymer arrays in mesoporous aluminavia simple drop-casting and appearance of anisotropic photoluminescence. Chemical Communications, 48(4), 549-551. https://doi.org/10.1039/C1CC14502A
13. Hu, B., Yao, M., Xiao, R., Chen, J., & Yao, X. (2014). Optical properties of amorphous Al2O3 thin films prepared by a sol–gel process. Ceramics International, 40(9, Part A), 14133-14139. https://doi.org/10.1016/j.ceramint.2014.05.148
14. Mäder, S., Haas, T., Kunze, U., & Doll, T. (2011). Ultrathin metal oxidation for vacuum monitoring device applications. physica status solidi (a), 208(6), 1223-1228. https://doi.org/10.1002/pssa.201000921
15. Dong, X., Jahanmir, S., & Hsu, S. M. (1991). Tribological Characteristics of α-Alumina at Elevated Temperatures. Journal of the American Ceramic Society, 74(5), 1036-1044. https://doi.org/10.1111/j.1151-2916.1991.tb04340.x
16. Senthil Kumar, A., Raja Durai, A., & Sornakumar, T. (2006). Wear behaviour of alumina based ceramic cutting tools on machining steels. Tribology International, 39(3), 191-197. https://doi.org/10.1016/j.triboint.2005.01.021
17. Park, N.-K., Choi, H.-Y., Kim, D.-H., Lee, T. J., Kang, M., Lee, W. G., Kim, H. D., & Park, J. W. (2013). Purification of Al(OH)3 synthesized by Bayer process for preparation of high purity alumina as sapphire raw material. Asian Crystallization Technology Symposium-2012, 373, 88-91. https://doi.org/10.1016/j.jcrysgro.2012.12.004
18. Kim, S.-M., Lee, Y.-J., Jun, K.-W., Park, J.-Y., & Potdar, H. S. (2007). Synthesis of thermo-stable high surface area alumina powder from sol–gel derived boehmite. Materials Chemistry and Physics, 104(1), 56-61. https://doi.org/10.1016/j.matchemphys.2007.02.044

19. Rehman Khan, H., & Arif Siddiqui, M. (2014). Effect of Milling Time on Al-Fe-Cr-20 Wt. % Al2O3composite Prepared Through Ball Milling. International Journal of Engineering Research and Applications, 4(7), 183-188.
20. Ramezani.M & T. Neitzert. (Decembre2012). Mechanical milling of aluminum powder using planetary ball milling process. Journal of Achievements in Materials and Manufacturing Engineering, 55(2), 790-798.
21. Mortazavi.A, M. Razavi, T. Ebadzadeh, & Ali Sedaghat Ahangari. (2016). Effect of milling time on the crystallite size and microstructure of Al2O3/Mo Nano composite. Advanced Ceramics Progress, 2(3), 12 16. https://doi.org/doi 10.30501/ACP.2016.70025
22. Salai Subha Nila, A., & Radha, K. P. (2018). Synthesis and XRD, FTIR Studies of Alumina Nanoparticle using Co-precipitation Method. International Journal for Research in Applied Science and Engineering Technology, 6(3), 2493-2496. https://doi.org/10.22214/ijraset.2018.3402
23. Wang, J., He, Q. N., & Gao, Z. (2011). The Effect of Different Solvent on the Microstructure of Gibbsite during Hydrothermal Treatment. Advanced Materials Research, 160-162, 76-80. https://doi.org/10.4028/www.scientific.net/AMR.160-162.76
24. CHEN.H, Xueye SUI, Changling ZHOU, Chonghai WANG, & Futian LIU. (2016). Preparation and characterization of monolithic Al2O3–SiO2 aerogel. Journal of the Ceramic Society of Japan, 124(4), 442 447. https://doi.org/10.2109/jcersj2.15184
25. Segal, F. M., Correa, M. F., Bacani, R., Castanheira, B., Politi, M. J., Brochsztain, S., & Triboni, E. R. (2018). A Novel Synthesis Route of Mesoporous γ-Alumina from Polyoxohydroxide Aluminum. Materials Research, 21(1), e20170674. https://doi.org/10.1590/1980-5373-MR-2017-0674
26. Saha, S. (1994). Preparation of alumina by sol-gel process, its structures and properties. Journal of Sol-Gel Science and Technology, 3(2), 117-126. https://doi.org/10.1007/BF00486718
27. Hosseini, S. A., Niaei, A., & Salari, D. (2011). Production of γ-Al2O3 from Kaolin. Open Journal of Physical Chemistry, 1(2), 23-27. https://doi.org/10.4236/ojpc.2011.12004
28. Roque-Ruiz, J. H., & Reyes-López, S. Y. (2016). Synthesis of α-Al2O3 Nanopowders at Low Temperature from Aluminum Formate by Combustion Process. Journal of Material Sciences & Engineering, 6(1), 305. https://doi.org/10.4172/2169-0022.1000305
29. Kaur,P, Khanna, A, Kaur, N, Nayar, P, & Chen, B. (2020). Synthesis and structural characterization of alumina nanoparticles. Phase Transitions, 93(6), 596 605. https://doi.org/10.1080/01411594.2020.1765245
30. Prashanth, P. A., Raveendra, R. S., Hari Krishna, R., Ananda, S., Bhagya, N. P., Nagabhushana, B. M., Lingaraju, K., & Raja Naika, H. (2015). Synthesis, characterizations, antibacterial and photoluminescence studies of solution combustion-derived α-Al2O3 nanoparticles. Journal of Asian Ceramic Societies, 3(3), 345-351. https://doi.org/10.1016/j.jascer.2015.07.001
31. Avci, N., Smet, P. F., Lauwaert, J., Vrielinck, H., & Poelman, D. (2011). Optical and structural properties of aluminium oxide thin films prepared by a non-aqueous sol–gel technique. Journal of Sol-Gel Science and Technology, 59(2), 327-333. https://doi.org/10.1007/s10971-011-2505-9
32. Manyasree, D., Kiranmayi, P., & Ravi Kumar, R. V. S. S. N. (2018). Synthesis, characterization and antibacterial activity of Aluminium Oxide nanoparticles. International Journal of Pharmacy and Pharmaceutical Sciences, 10(1), 32-36. https://doi.org/10.22159/ijpps.2018v10i1.20636

33. Reyes, J. M., Perez Ramos, B. M., Islas, C. Z., Arriaga, W. C., Quintero, P. R., & Jacome, A. T. (2013). Chemical and Morphological Characteristics of ALD Al2O3 Thin-Film Surfaces after Immersion in pH Buffer Solutions. Journal of The Electrochemical Society, 160(10), B201. https://doi.org/10.1149/2.060310jes
34. Djebaili, K., Mekhalif, Z., Boumaza, A., & Djelloul, A. (2015). XPS, FTIR, EDX, and XRD Analysis of Al2O3 Scales Grown on PM2000 Alloy. Journal of Spectroscopy, 2015(1), 868109. https://doi.org/10.1155/2015/868109
35. Dhawale, V. P., Khobragade, V., & Kulkarni, S. D. (2018). Synthesis and Characterization of Aluminium Oxide (Al2O3) Nanoparticles and its Application in Azodye Decolourisation. International Journal of Environmental Chemistry, 2(1), 10-17. https://doi.org/10.11648/j.ijec.20180201.13
36. Sobhani, M., Tavakoli, H., Chermahini, M. D., & Kazazi, M. (2019). Preparation of macro-mesoporous γ-alumina via biology gelatin assisted aqueous sol-gel process. Ceramics International, 45(1), 1385-1391. https://doi.org/10.1016/j.ceramint.2018.09.056
37. Qin, H., Guo, W., & Xiao, H. (2019). Preparation of γ-Al2O3 membranes for ultrafiltration by reverse micelles-mediated sol-gel process. Ceramics International, 45(17, Part B), 22783-22792. https://doi.org/10.1016/j.ceramint.2019.07.320
38. Fakhimi, O., Najafi, A., & Khalaj, G. (2020). A facile rout to obtain Al2O3 nanopowder via recycling aluminum cans by sol-gel method. Materials Research Express, 7(4), 045008. https://doi.org/10.1088/2053-1591/ab8653
39. Santos, R. C. R., Pinheiro, A. N., Leite, E. R., Freire, V. N., Longhinotti, E., & Valentini, A. (2015). Simple synthesis of Al2O3 sphere composite from hybrid process with improved thermal stability for catalytic applications. Materials Chemistry and Physics, 160, 119-130. https://doi.org/10.1016/j.matchemphys.2015.04.014
40. Omer, A. H., Bin Mokaizh, A. A., & Shariffuddin, J. H. B. H. (2021). Low-calcination Temperature to Synthesize A-Alumina From Aluminium Waste Can Using Sol-Gel Method. IOP Conference Series: Earth and Environmental Science, 641(1), 012023. https://doi.org/10.1088/1755-1315/641/1/012023